Defect-induced homogeneous amorphization of silicon: the role of defect structure and population

2006 J. Phys.: Condens. Matter 18 2077

(http://iopscience.iop.org/0953-8984/18/6/020)

INSTITUTE OF PHYSICS PUBLISHING JOURNAL OF PHYSICS: CONDENSED MATTER

J. Phys.: Condens. Matter **18** (2006) 2077–2088 doi:10.1088/0953-8984/18/6/020

Defect-induced homogeneous amorphization of silicon: the role of defect structure and population

Giorgio Lulli[1], **Eros Albertazzi**[1], **Simone Balboni**[2] **and Luciano Colombo**[3]

[1] Consiglio Nazionale delle Ricerche, Istituto per la Microelettronica e i Microsistemi, Sezione di Bologna, Via P Gobetti 101, I-40129 Bologna, Italy
[2] CeSIA—Settore Reti e Comunicazioni, Università di Bologna, Viale Filopanti 3, I-40126 Bologna, Italy
[3] SLACS (CNR–INFM) and Dipartimento di Fisica, Università degli Studi di Cagliari, Cittadella Universitaria, I-09042 Monserrato (Cagliari), Italy

E-mail: lulli@bo.imm.cnr.it

Received 11 October 2005, in final form 9 January 2006
Published 27 January 2006
Online at stacks.iop.org/JPhysCM/18/2077

Abstract

Molecular dynamics based on the environment-dependent interatomic potential is used to investigate the influence of the nature and distribution of defects on solid state, homogeneous amorphization of Si. To this end, different kinds of defects, including single interstitials and vacancies (both uncorrelated and correlated distributions), bond defects, and small interstitial and vacancy clusters, have been considered. It is shown that the threshold defect concentration for amorphization depends on the defect type, and, in the case of single defects, on the degree of correlation between interstitial and vacancy distributions. The threshold varies within the interval [0.18–0.28] atomic fraction, the upper value corresponding to the case of bond defects, the lower to the uncorrelated distributions of single ⟨110⟩ split interstitials plus compensating vacancies.

1. Introduction

Depending on irradiation conditions (temperature, particle energy, mass, fluence, and flux) crystalline Si (c-Si) may transform into amorphous Si (a-Si) under bombardment with energetic particles. Ion beam-induced amorphization of Si, an issue which has important consequences for applications such as dopant implantation or defect engineering in Si-based microelectronics, has been recently reviewed in [1]. The physical mechanism of such a phase change, as well as its actual pathway, critically depends both on experimental conditions and on the details of processes (defect generation, diffusion, recombination, and clustering) which elude direct experimental observation. The two simple schemes traditionally adopted for describing this process are the heterogeneous model [2, 3], in which amorphization occurs as the result of the overlapping of microscopic amorphous regions created by individual ion impacts [2, 3],

and the homogeneous model [4, 5], in which amorphization occurs when the concentration of defects reaches the value for which the free energy of the disordered crystal exceeds the free energy of a-Si. In recent years, atomic scale computational methods allowed for a thorough investigation of the above phenomena, improving our basic understanding and providing a picture which is more complex than previously guessed from either the pure homogeneous or heterogeneous models. Molecular dynamics (MD) based on classical model potentials [6–8] has shown that heterogeneous nucleation of amorphous clusters plays the dominant role in low temperature, heavy-ion irradiation, whereas the homogeneous mechanism is dominant in amorphization induced by high temperature, light-particle irradiation.

An important parameter of the homogeneous model is the threshold concentration of defects for which the system undergoes a crystal-to-amorphous (c–a) phase transition. This parameter appears, for instance, in phenomenological models of damage accumulation used in the simulation of the ion implantation process using the Monte Carlo binary collision approximation (MC-BCA). The subject has been investigated by performing ideal computer experiments in which, after the introduction of a definite concentration of defects, the system is then aged by a MD annealing at relatively high temperature [9–15]. Issues affecting the amorphization threshold are the model potential, the defect types, and the way the defects are spatially distributed. In a few cases, interstitials and vacancies [11, 12] and the Stillinger–Weber (SW) [16] potential were used. More recent investigations [1, 13–15, 17] have focused on the role of the bond defect (bd), or I–V pair [18, 19], using the Tersoff (TS) [20] model potential. Most of these studies have investigated the behaviour of constant, homogeneous distribution of defects or Frenkel pairs. In some cases it has also been shown how the degree of agglomeration of bd [1, 14, 15] or the presence of an amorphous phase in contact with a disordered crystal [11] may influence the evolution of the disordered phase towards either amorphization or crystallization.

In the present work we report a study of defect-induced homogeneous c–a transformation in Si, using MD and the environment-dependent interatomic potential (EDIP [21, 22]), a model known to give a good description of local bonding in bulk defects and disordered phases of Si. The purpose is to show how the threshold defect concentration for the solid state c–a transition varies with the varying nature of primarily introduced defects, a matter not investigated in previous works. Defects used to model disorder include different configurations of interstitials (I) plus compensating vacancies (V) (uncorrelated and correlated distributions), bd, and small V and I clusters. The results of this study can, we hope, give a more comprehensive picture of homogeneous amorphization than analyses based on a single defect type.

2. Method

2.1. Preparation of Si supercells with defects

Si supercells of size $10 \times 10 \times 10$ lattice units (1 lattice unit $= 0.5431$ nm) were populated with constant concentrations of defects. The population algorithm prevents defect overlapping, thus ensuring that defects in the initial state are separated. Any recombination and clustering is therefore the consequence of the MD cycle. The models of the split interstitials $\langle 110 \rangle$ (I_S), the tetrahedral (I_T) interstitials, the hexagonal (I_H) single interstitials, and the di-interstitial (I_2) and tri-interstitial (I_3) clusters obtained from tight-binding molecular dynamics (TBMD) simulations [23] were considered in this work. An equal amount of vacancies, introduced as single point defects (V) or small clusters (V_n, with $n = 2, 3$), is always introduced to compensate for the interstitials and keep the number of atoms constant in the supercell. By default, the distributions of vacancy-type and interstitial-type defects are random and

uncorrelated. In the case of the $I_S + V$ and $I_H + V$ distribution, we have also investigated the role of defect correlation, by populating the supercell with I–V pairs instead of independent I and V distributions. In this case the correlation radius (C_r) is the maximum distance allowed between the two elements of each pair.

In previous works [1, 13–15, 17, 24, 25], the accumulation of bd was investigated as the mechanism of amorphization of Si. Introduced as an artificial topological defect for the purpose of computer generation of a-Si [24], in recent years the bd has been identified by simulation as a defect which may occur in Si either as the result of incomplete vacancy–interstitial recombination [18] or as a primary radiation defect [17]. Its properties were investigated by first-principles methods [19], from which it was found that the bd has a formation energy lower than other elementary point defects in Si. The results of [18, 19] have been further confirmed by more recent investigations [26]. Moreover, it was estimated that bd, unlike single vacancies and interstitials, can be stable for a relatively long time ($\sim\mu$s) at room temperature [13]. For comparison purposes, the bd has also been considered in the present study. Since no excess atoms are introduced by this defect, no compensating vacancies are needed in this case.

Initial lattice coordinates of defects were taken from configurations calculated from TBMD in 512-atom Si cells [23]. More details on the preparation of defect-containing Si supercells are reported in previous works [27, 28].

2.2. Molecular dynamics simulation

The aim of MD simulation is to determine whether a supercell populated with a constant, homogeneous concentration of defects will evolve into a perfect crystal or into a fully disordered (amorphous) state, once a sufficient thermal budget is supplied. The criterion of stable amorphization is met when: (i) the potential energy of the disordered phase, annealed at a relatively high temperature (1000 K in our case), reaches an almost stationary state, well above the energy of the crystal, and stable for at least 1 ns; (ii) this state, after cooling to 300 K and equilibration, shows structural properties (pair correlation function, average coordination) characteristic of the amorphous Si phase. The annealing temperature of 1000 K was selected taking into account the EDIP-provided value for melting temperature of Si in both crystalline and amorphous phases [29]. As a matter of fact, at $T = 1000$ K the crystalline (or defect-containing) sample is still well within the solid state phase, and any microstructure evolution observed during present MD runs is not due to self-diffusion liquid-like phenomena. Rather, it is strictly related to interactions among defects. The standard time cycle used in this work consists of an instantaneous temperature rise up to $T = 1000$ K, followed by 0.8 ns annealing at 1000 K, 0.2 ns cooling down to $T = 0$ K, and a final 0.02 ns relaxation. This cycle was applied to all different defects and initial concentrations investigated. Although at this time the different behaviour due to different defects is already well characterized (see the results below), the annealing is too short to determine whether the system meets the criterion for stable amorphization stated above. To overcome this limitation, supercells populated with near-threshold defect concentrations were annealed for longer times, up to a maximum of 8 ns. This allowed more quantitatively reliable estimations of amorphization thresholds.

To gently reduce the energy of the system before MD annealing, defective supercells were subjected to 500 preliminary steps of structural relaxation at vanishing temperature. Simulations were performed in the bulk, using periodic boundary conditions in the three spatial coordinates. Results reported in the following were obtained using the NVT ensemble as a default. NPT (zero pressure, Andersen barostat) conditions were also adopted in some selected cases, to check their possible influence on the crystal-to-amorphous transition. The time step for the integration of motion equations was 2×10^{-15} s. To investigate the dependence

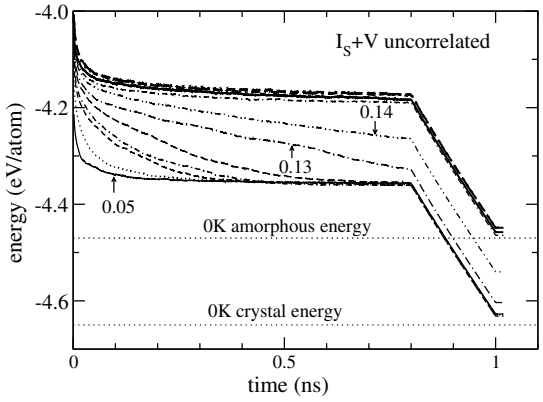

Figure 1. Potential energy evolution of supercells populated with different concentrations of uncorrelated $I_S + V$ defects during the MD–EDIP annealing cycle (1000 K for 0.8 ns followed by 0.2 ns cooling to 0 K and 0.02 ns relaxation at 0 K). The increasing values of concentration corresponding to the curves reported in the figure are 0.05, 0.08, 0.10, 0.11, 0.12, 0.13, 0.14, 0.15, 0.16, 0.20, 0.30, 0.40 atomic fraction.

of the results on the annealing temperature, some runs were also performed at $T = 1150$ K, a value still well below the melting point of Si.

3. Results and discussion

3.1. Uncorrelated point defect distributions

As an example, figure 1 shows the potential energy versus time evolution during the standard 1000 K MD cycle (NVT ensemble) for different initial concentrations of randomly distributed and uncorrelated $I_S + V$ defects. Similar runs were performed for $I_H + V$, $I_T + V$ and bd distributions, and the energies both after population plus relaxation (upper curves) and after an MD cycle plus a quench (lower curves) are reported in figure 2 as a function of the initial concentration of defects. Statistical uncertainties of results (error bars in the figure) were evaluated via multiple runs using different sequences of pseudo-random numbers in the defect population algorithm. The variance is rather small ($\leqslant 10^{-2}$ eV) for conditions well below and well above the regions where the curves rise, whereas is larger (up to $2–3 \times 10^{-2}$ eV) for defect concentrations which fall close to the transition regions.

Data of figure 2 clearly indicate that the threshold defect concentration which separates crystallization and amorphization regimes depends on the defect type. On the other hand, figure 1 shows that after 0.8 ns at 1000 K, the potential energy of supercells is in most cases still decreasing, even for concentration values well above the rising point of the curves in figure 2. To investigate this issue, a series of 8 ns cycles (not shown) were run. As mentioned previously, amorphization is assumed to occur if the energy reaches a typical value (~ -4.2 eV/atom at 1000 K for the EDIP) which remains stable for at least 1 ns. According to this criterion, we estimated the following threshold concentrations: 0.18 ± 0.01 atomic fraction in the case of $I_S + V$, 0.21 ± 0.01 in the case of $I_H + V$ and $I_T + V$, 0.28 ± 0.01 in the case of bd. The comparison of these values with the apparent transition regions of the curves in figure 2, indicates that an annealing for $\gg 8$ ns is necessary for reliably estimating the threshold for stable amorphization. It was found that the above results do not change on using the NPT ensemble at constant zero pressure. To further check the influence of temperature, NVT runs

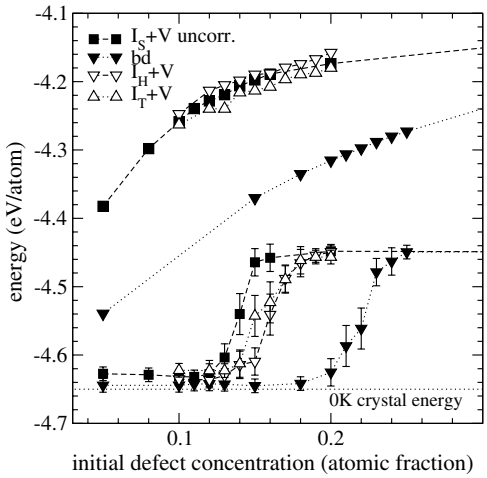

Figure 2. Potential energy of the supercells after defect population and 0 K relaxation (upper curves) and after an MD cycle and a quench (lower curves), reported as a function of the initial concentration of uncorrelated $I_S + V$, $I_T + V$, $I_H + V$ and bd.

at 1150 K were also performed for both bd and $I_S + V$ populations. No sizable difference from the thresholds determined with the 1000 K cycle was observed.

The threshold determined for supercells populated with bd is slightly higher than previous results based on the Tersoff force field [9, 13], whereas the value determined for the $I_T + V$ distribution is lower than that found in [12], using the SW model potential. This is probably a consequence of the stronger tendency in the SW model for reconstruction of the tetrahedral symmetry of c-Si in comparison with the EDIP or TS potential cases [8].

The amorphization threshold can be influenced both by energetics and kinetics, in particular the competition between defect clustering and recombination. A full characterization of defect kinetics by means of MD–EDIP is beyond the scope of the present work; however, in order to better understand some observed trends in amorphization, we performed some MD cycles on supercells containing a few I–V pairs only. The main results of these observations are the following: (i) an I–V encounter can lead either to defect annihilation or to the formation of a bd, according to a mechanism very similar to the one originally discovered from TBMD simulations [18]; (ii) once formed, a bd remains immobile at 1000 K and can survive for times up to $\sim$1 ns, before annealing by bond switching. The upper curves reported in figure 2 show that, just after defect insertion and relaxation, there is no appreciable difference in energy of supercells populated with I_H+V, I_T+V and I_S+V. The differences in amorphization thresholds observed from MD should then be ascribed to differences in defect kinetics. We found that the relative probabilities of pair annihilation or bd formation upon I–V encounters depend on the interstitial type and on the direction of I–V approach. In particular, there is a high chance of bd formation for close I_S–V pairs in which the vacancy occupies one of the two neighbour sites lying along the direction perpendicular to the dumb-bell. Such a probability is significantly lower for close I_S–V pairs where the vacancy is in one of the two sites in the direction parallel to the dumb-bell, and all possible configurations of close I_H–V and I_T–V pairs. Due to the remarkable stability of bd, a higher probability of formation of this defect, as compared to I–V annihilation, acts as a mechanism of damage stabilization; this can explain the slightly higher amorphization threshold observed for $I_S + V$, in comparison with $I_H + V$ and $I_T + V$ defect population.

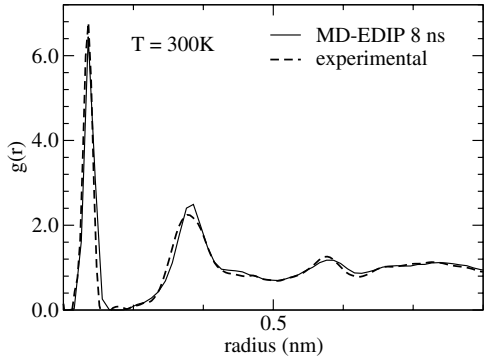

Figure 3. Pair correlation functions of supercells with the initial concentration of 0.2 atomic fraction of $I_S + V$, after the long (8 ns) 1000 K treatment plus quench, and subsequent equilibration at 300 K. The curve relating to the computational sample is compared with the experimental, room temperature $g(r)$ of well relaxed amorphous Si produced by ion implantation and low temperature annealing [30, 31].

On the other hand, the lower initial energy of supercells containing bd in comparison with those populated with I + V (see the upper curves in figure 2) is the main reason for the lower amorphization threshold observed in the latter case. From the point of view of kinetics, V–V and I–I clustering contributes to keeping the energy and the disorder of supercells populated with I + V distributions above those of supercells populated with bd during annealing.

For defect concentrations above the threshold, the system evolves towards a fully disordered state with an energy after 8 ns long annealing, a good 0.18 eV/atom above the energy of the crystal, and with properties independent both of the nature and of the initial concentration of defects. Quench rates up to four times slower than the standard 5000 K ns^{-1} were also tested, but they were not found to affect the properties of the final state. NPT simulations gave for this phase an amorphous/crystal density ratio equal to 0.97 and an average coordination (calculated with a bond cut-off radius of 0.3 nm) of 4.07. The pair correlation function $g(r)$ at 300 K, calculated with 8 ns cycles from an initial distribution of 0.20 $I_S + V$, is in fairly good agreement with the experimental $g(r)$ of well relaxed amorphous Si [30, 31], as shown in figure 3. The small differences in location of the peaks are similar to those reported in a recent study [32] performed with the TS potential, and reflect the difference between simulated and experimental coordination numbers; the latter is 3.88 for the experiment reported in figure 3.

An intermediate state, appearing as a heterogeneous mix of heavily damaged and nearly crystalline domains, is observed after 0.8 ns for defect concentrations in between 0.12 and 0.16 in the case of $I_S + V$, and 0.22 and 0.24 in the case of bd. This can be seen in figure 4, which shows ⟨100⟩ views of annealed and quenched supercells with initial $I_S + V$ concentrations (a) below, (b) close to, and (c) above the transition threshold. Configurations such as the one in figure 4(b) evolve as a result of intrinsic statistical fluctuations in defect concentration and damage coarsening mechanisms and clearly represent unstable states, as shown by the strongly negative slope of the energy versus time curves after 0.8 ns (figure 1). These configurations are observed to decrease their energy and disorder upon further annealing, until a final state similar to the one shown in figure 4(a) is eventually reached after several ns. Their instability at the relatively high temperature of 1000 K does not exclude the possibility that they can survive for a very long time at lower temperature. As an example, the configuration of figure 4(b) was further annealed for 8 ns at 700 and 300 K. While its energy is found to decrease continuously

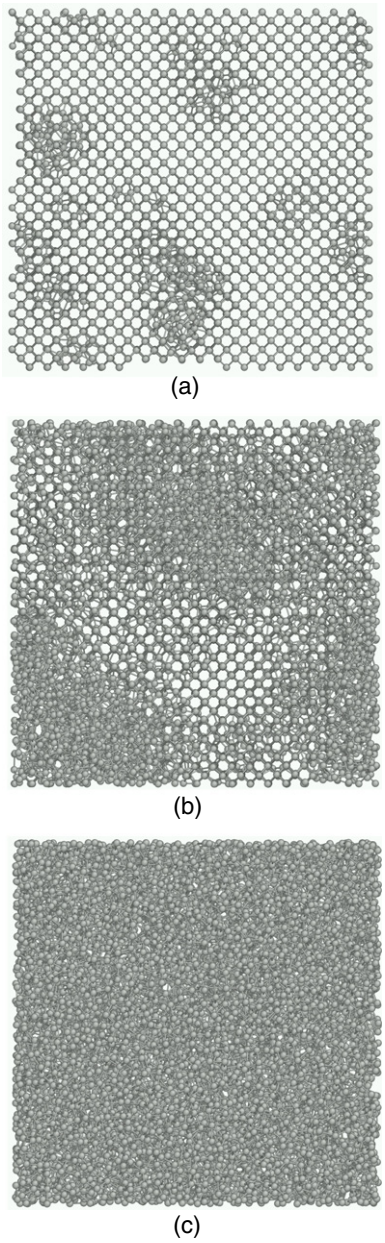

Figure 4. ⟨100⟩ views of supercells with different initial concentrations of uncorrelated I_S+V defects, after the standard 0.8 ns at 1000 K MD cycle plus quench to 0 K. Initial defect concentrations: (a) 0.05, (b) 0.14, (c) 0.2 atomic fraction. (This figure was produced with the free software AtomEye [38].)

also during 700 K annealing, indicating that it would recrystallize at times $t \gg 8$ ns, no change at all, either in energy or in structure, is observed after 8 ns at 300 K.

3.2. Correlation in the point defect distribution

Results of figure 2 show that the threshold for solid state, defect-induced homogeneous amorphization of Si depends on the nature of defects introduced in the lattice. In particular, a large difference is found between the cases involving I (I_S, I_H, I_T) + V defects, on one hand, and an bd population, on the other.

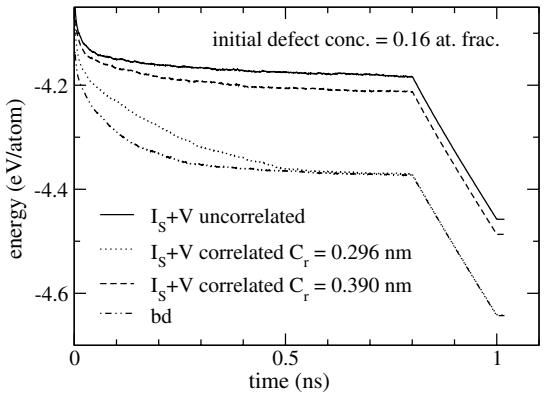

Figure 5. Effect of correlation in I_S and V distributions on the potential energy evolution versus time, in the case of an initial defect concentration of 0.16 atomic fraction. The correlation radius C_r is the maximum distance allowed between I_S and V in each Frenkel pair.

Although MD simulations [17] have shown that the bd can also be generated as a primary radiation defect in Si, its main formation mechanism is likely to be by I–V coupling [18]. As described in the previous section, the formation of bd may be observed using MD–EDIP as an intermediate step to I–V recombination, its probability depending on the defect type and direction of I–V approach. If bd is basically the product of I–V coupling, a homogeneous distribution of such defects can be thought of as the result of the evolution of a I+V distribution with strong correlation between I and V, i.e. a distribution where each vacancy is much closer to the interstitial originating from the same displacement event than to other defects. Under these conditions, the probability of I–V interaction (and therefore of either bd formation or I–V annihilation) is much larger than the probability of V–V or I–I clustering. A distribution of correlated I–V is expected to better represent the experimental situation encountered during electron beam irradiation. In fact, in this case, individual scattering events producing lattice defects are well separated in space, whereas the energy transferred in nuclear collisions is typically low. Under these conditions, the majority of primarily induced defects can be assumed to be correlated I–V pairs which are found close one another after the recoil atom has dissipated the low momentum gained from the energetic electron. Correlation was introduced in $I_S + V$ and $I_H + V$ distributions, as described in section 2.1, and simulations for different values of C_r were performed. Two kinds of distributions were considered due to the different probabilities for bd formation, as pointed out in the previous section. The behaviour of $I_T + V$, not reported, was found very similar to that of $I_H + V$.

As an example of the correlation effect, figure 5 shows the potential energy versus time for both uncorrelated and correlated $I_S + V$ distributions, for the case of an initial defect concentration of 0.16 atomic fraction. The results corresponding to the same initial concentration of uncorrelated $I_S + V$ and bd are reported for comparison. As expected, I–V correlation increases the probability of defect annealing, thus increasing the amorphization threshold as well. At the relatively high defect concentration of 0.16, the effect of correlation is large just in the case where the vacancy is a first neighbour of the interstitial ($C_r = 0.239$ nm).

Figure 6 reports the full transition curve of the strongly correlated ($C_r = 0.239$ nm) $I_S + V$ and $I_H + V$ distributions, compared to the curves for uncorrelated $I_S + V$ and bd. The energy after the preliminary static optimization decreases upon the introduction of defect correlation. It is lower for correlated $I_S + V$ pairs than for $I_H + V$, but in both cases remains well above the energy introduced by bd.

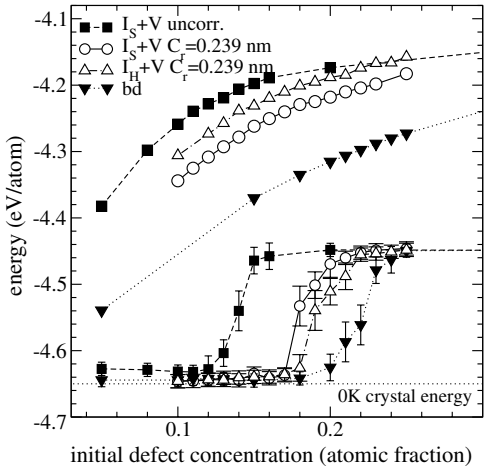

Figure 6. Effect of I–V correlation on the transition between crystallization and amorphization regimes.

After 0.8 ns of annealing, for defect concentrations below the transition to amorphous, the final energies (and residual defect concentrations) of supercells populated with strongly correlated I + V are equal, within the statistical uncertainty, to those populated with bd. As the defect concentration increases above $\simeq$0.17–0.19 atomic fraction, the damage after MD for correlated I_S + V and I_H + V distributions suddenly increases, leading in both cases to a lower amorphization threshold. The excess energy of I–V pairs in comparison with bd, the larger strain introduced in the lattice, and the consequent stronger increase in mutual interaction upon increasing concentration are the probable reasons for the collapse of the crystal structure occurring at a lower defect concentration. Moreover, it is observed that, despite the higher initial energy, correlated I_H + V pairs give a slightly higher threshold than I_S + V. In this case defect kinetics, in particular the different probability of close pair I–V annihilation in comparison with bd formation, already discussed in the previous section, is responsible for the observed difference.

3.3. Population with point defect clusters

To investigate the effect of introducing small clusters in place of single defects, supercells were populated with distributions of I_2 and I_3 defects, compensated by uncorrelated distributions of vacancies. The latter can be in the form of single V, V_2, or V_3 clusters. The structural models of I_2 and I_3, once again determined by means of TBMD [23], are the same as those described in [28]; V_2 and V_3 are obtained by simply removing two neighbour lattice atoms, and one atom and two neighbours, respectively.

Figures 7 and 8 show the transition curves of the supercells populated with I_2 and I_3, respectively, compensated with V, V_2, or V_3 defects. These data are compared with the transition curves of the uncorrelated I_S + V and bd distributions. An effect of introducing defect clusters and increasing their size is the decrease of the initial energy of supercells. This effect is not large and its amount varies from case to case. On the other hand, a significant increase in the amorphization threshold is observed with increasing size of clusters. Amorphization thresholds found for population with I_2 and I_3 clusters fall within the interval bounded on the lower side by uncorrelated I_S + V and on the upper side by bd distributions.

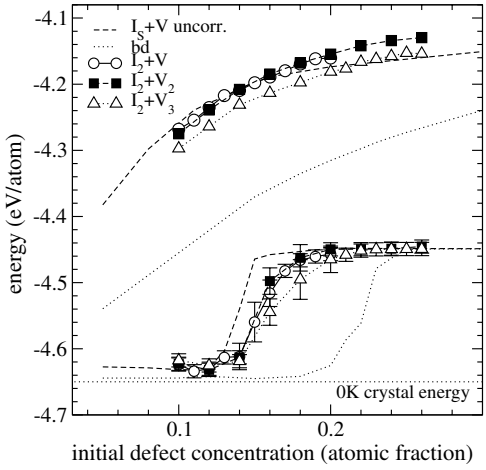

Figure 7. Effects of the population with interstitial and vacancy clusters (uncorrelated distributions) on the transition between crystallization and amorphization regimes: the case of I_2.

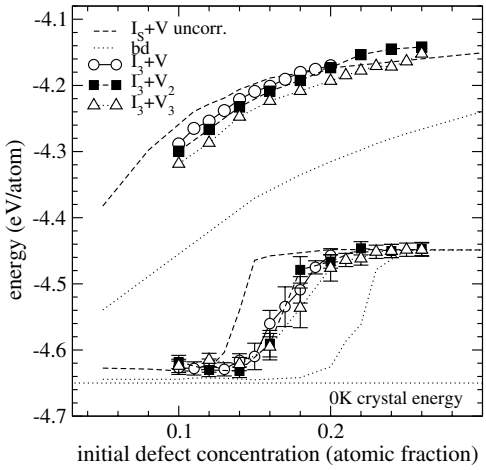

Figure 8. Effects of the population with interstitial and vacancy clusters (uncorrelated distributions) on the transition between crystallization and amorphization regimes: the case of I_3.

Since the differences in initial energies seem in some cases too small to determine the observed shift in the transition, we have looked in more detail at the defect kinetics. To this end we followed the dynamics of single, isolated defect clusters, and observed that vacancy clusters V_n, $n = 1, 3$, do not move on the timescale of $\sim$1 ns, whereas I_2 and I_3 have mobilities very close to that of I_S. Such a high mobility is probably the cause of the increase in the amorphization threshold. If we consider each cluster as one defect and keep the total number of I (and V) constant, the concentration of defects is smaller when populating with I_2 and I_3 than when populating with I_S. For a lower concentration of larger objects with similar mobility, it may be expected that the recombination due to encounters between I and V aggregates, each containing more than one defect, will lead to a higher rate of defect removal, and therefore to an increase in the amorphization threshold. The result is then influenced by the mobility of clusters, which depends on the model potential. Recent temperature-accelerated TBMD simulations have shown that I_2 has a diffusivity comparable to the mono-interstitial in Si over a wide temperature range [33]. For I_3, apparently contrasting results have been obtained [33, 34]. The relative mobility of interstitial clusters compared to single interstitials, as determined using MD–EDIP, appears in agreement with TBMD findings for I_2, whereas it could be overestimated (according to [33]) for I_3. In the latter case the

homogeneous amorphization threshold for supercells populated with I_3 could be overestimated as well.

4. Connection with experiments

Due to the idealized conditions under which MD simulations are performed, it is not easy to make a direct comparison with irradiation experiments. In reality, out-of-equilibrium, non-homogeneous configurations of lattice damage (such as the one schematized in figure 4(b)) can survive at low temperature and accumulate on a timescale that is $\gg$8 ns, as an effect of prolonged irradiation. These and other effects are not considered in the simple simulation scheme used here. Nevertheless, if we refer to conditions which better approximate homogeneous defect generation, i.e. irradiation with swift light ions, or electrons, the results reported here represent a useful reference for the interpretation of experiments.

A clear experimental demonstration of purely homogeneous amorphization of Si is still lacking. Even for electron beam-induced amorphization, observed during low temperature, *in situ* irradiation in the transmission electron microscope [35], it has been hypothesized that the presence of embryos in the form of small interstitial clusters is necessary to trigger the crystal-to-amorphous transition [36]. The interpretation of these experiments is complicated by effects such as ionization-enhanced defect diffusion [37] and the presence of surfaces, defect sinks, and traps which may considerably alter the defect kinetics, favouring defect annealing in comparison with clustering, and thus making the amorphization conditions more difficult to reach.

What we have shown in this work is that the defect concentration leading to lattice amorphization may vary depending on the nature of defects introduced in the lattice and on the way they are distributed. In comparison with previous works, which focused on the case of a single defect type, our results, we hope, give a more comprehensive picture of the phenomenon, allowing a more conservative estimate of the amorphization threshold, a physical parameter very important for predicting the stability of the Si lattice upon irradiation.

5. Conclusion

In this work it is shown that the threshold defect concentration for homogeneous solid state, defect-induced amorphization of Si, as modelled by MD–EDIP, depends on the nature of defects, and on the way they are distributed in the lattice. As regards the latter issue, the investigation considers the effects of I–V correlation and of the introduction of small I_n ($n = 2, 3$) and V_n ($n = 2, 3$) clusters in place of single defects, while assuming in all cases a constant, homogeneous distribution of individual defects or Frenkel pairs. In general, both energetics and kinetics influence the amorphization threshold: this usually increases as the energy introduced in the supercell by defect population decreases. However, defect kinetics (competition between defect recombination and clustering, or bd formation) appears in some cases the main factor responsible for the different thresholds observed for different initial defect distributions. The threshold defect concentration for amorphization was found to be within the interval [0.18–0.28] atomic fraction, the upper value corresponding to the case of bd, the lower to the totally uncorrelated $I_S + V$ distribution. Increasing the correlation between I and V increases the amorphization threshold. This is due to the increasing probability of I–V encounters in comparison with I–I or V–V clustering. In the case of maximum correlation (all V first neighbours of I), the crystal–amorphous transition curves undergo an appreciable shift towards the curve corresponding to the bd population, but the amorphization thresholds remain lower. This is a consequence of the higher energy and strain introduced by strongly correlated

I–V pairs in comparison with bd. The case of bd gives therefore an ideal upper estimate of the threshold defect concentration for homogeneous amorphization of Si. Populating with small defect clusters ($I_{2,3}$, $V_{2,3}$) increases the threshold to above the one observed for single-defect distributions. This effect is probably influenced by the high mobility of I_2 and I_3, as foreseen by means of MD–EDIP.

Acknowledgments

This work was partially supported by the FIRB national project (contract RBAU01LLX2). S Roorda is acknowledged for supplying the experimental pair correlation function for amorphous Si shown in figure 3.

References

[1] Pelaz L, Marquès L A and Barbolla J 2004 *J. Appl. Phys.* **96** 5947
[2] Morehead J F F and Crowder B L 1970 *Radiat. Effects* **6** 27
[3] Gibbons J F 1972 *Proc. IEEE* **60** 1062
[4] Dennis J R and Hale E B 1978 *J. Appl. Phys.* **49** 1978
[5] Holland W, Pennycook S J and Albert G L 1989 *Appl. Phys. Lett.* **55** 2503
[6] de la Rubia T D and Gilmer G H 1995 *Phys. Rev. Lett.* **74** 2507
[7] Caturla M J, DiazdelaRubia T, Marques L A and Gilmer G H 1996 *Phys. Rev.* B **54** 16683
[8] Nordlund K, Ghaly M, Averback R S, Caturla M, DiazdelaRubia T and Tarus J 1998 *Phys. Rev.* B **57** 7556
[9] Motooka T 1994 *Phys. Rev.* B **49** 16367
[10] Colombo L and Maric D 1995 *Europhys. Lett.* **29** 623
[11] Lewis L J and Nieminen R M 1996 *Phys. Rev.* B **54** 1459
[12] Barone M E and Maroudas D 1997 *J. Comp. Aid. Mater. Des.* **4** 63
[13] Marqués L A, Pelaz L, Hernández J, Barbolla J and Gilmer G H 2001 *Phys. Rev.* B **64** 045214
[14] Marquès L A, Pelaz L, Aboy M, Enriquez L and Barbolla J 2003 *Phys. Rev. Lett.* **91** 135504
[15] Pelaz L, Marquès L A, Aboy M and Barbolla J 2004 *Nucl. Instrum. Methods Phys. Res. B* **216** 41
[16] Stillinger F H and Weber T A 1985 *Phys. Rev.* B **31** 5262
[17] Stock D M, Weber B and Gärtner K 2000 *Phys. Rev.* B **61** 8150
[18] Tang M, Colombo L, Zhu J and DiazdelaRubia T 1997 *Phys. Rev.* B **55** 14279
[19] Cargnoni F, Gatti C and Colombo L 1998 *Phys. Rev.* B **57** 170
[20] Tersoff J 1988 *Phys. Rev.* B **37** 6991
[21] Bazant M Z, Kaxiras E and Justo J F 1997 *Phys. Rev.* B **56** 8542
[22] Justo J F, Bazant M Z, Kaxiras E, Bulatov V V and Yip S 1998 *Phys. Rev.* B **58** 2539
[23] Colombo L 2002 *Annu. Rev. Mater. Res.* **32** 271
[24] Wooten F, Winer K and Weaire D 1985 *Phys. Rev. Lett.* **54** 1392
[25] Motooka T 1996 *Thin Solid Films* **272** 235
[26] Goedecker S, Deutsch T and Billard L 2002 *Phys. Rev. Lett.* **88** 235501
[27] Balboni S, Albertazzi E, Bianconi M and Lulli G 2002 *Phys. Rev.* B **66** 045202
[28] Lulli G, Albertazzi E, Bianconi M, Satta A, Balboni S and Colombo L 2004 *Phys. Rev.* B **69** 165216
[29] Brambilla L, Colombo L, Rosato V and Cleri F 2000 *Appl. Phys. Lett.* **77** 2337
[30] Laaziri K, Kycia S, Roorda S, Chicoine M, Robertson J L, Wang J and Moss S C 1999 *Phys. Rev. Lett.* **82** 3460
[31] Laaziri K, Kycia S, Roorda S, Chicoine M, Robertson J L, Wang J and Moss S C 1999 *Phys. Rev.* B **60** 13520
[32] Izumi S, Hara S, Kumagai T and Sakai S 2004 *Comput. Mater. Sci.* **31** 258
[33] Cogoni M, Uberuaga B P, Voter A F and Colombo L 2005 *Phys. Rev.* B **71** 121203 (R)
[34] Du Y A, Barr S A, Hazzard K R A, Lenosky T J, Hennig R G and Wilkins J W 2005 *Phys. Rev.* B **72** 241306
[35] Takeda S and Yamasaki J 1999 *Phys. Rev. Lett.* **83** 320
[36] Yamasaki J, Takeda S and Tsuda K 2002 *Phys. Rev.* B **65** 115213
[37] Bourgoin J C and Corbett J W 1978 *Radiat. Effects* **36** 157
[38] Li J 2003 *Modelling Simul. Mater. Sci. Eng.* **11** 173